Published in "Physica C: Superconductivity 505: 32–38, 2014"
which should be cited to refer to this work.

Enhanced superconducting properties of rare-earth oxides and graphene oxide added MgB_2

Sudesh [a], S. Das [b], C. Bernhard [b], G.D. Varma [a,*]

[a] Department of Physics, Indian Institute of Technology Roorkee, Roorkee 247667, Uttarakhand, India
[b] Department of Physics and Fribourg Centre for Nanomaterials-FriMat, University of Fribourg, Chemin du Musee 3, CH-1700 Fribourg, Switzerland

In this paper, the effects of addition of (i) graphene oxide (GO), (ii) a series of rare-earth (RE, RE = La, Sm, Eu, Gd, Tb and Ho) oxides (REO) and (iii) a mixture of GO and rare-earth oxides (GO + REO) on the superconducting properties of MgB_2, have been studied with the help of electrical transport and magnetic measurements. All the samples have been prepared following the standard solid-state reaction route. We have used an optimum value of 1 wt% REO and 3 wt% GO for addition on the basis of previous studies. X-ray diffraction studies confirm the formation of hexagonal crystal structure (space group P6/mmm) of MgB_2 with small amounts of REB_x (x = 4 and 6) and MgO impurity phases in all the synthesized samples. We observe that the critical current density, J_c and upper critical field $H_{c2}(0)$ improve significantly in the REO-added and GO-added samples with no significant change in critical temperature, T_c. A substantial enhancement in $J_c(H)$ and $H_{c2}(0)$ is observed with the GO + REO addition in MgB_2. The different flux pinning mechanisms in all the samples are studied and it is found that the point pinning is the dominant mechanism in the GO-added samples and grain boundary pinning is the dominant one in the REO added samples. We have seen the combined effect of both types of flux pinning mechanisms in GO + REO added MgB_2.

1. Introduction

With its high critical temperature of 39 K [1], MgB_2 presents a potential material for technological applications. Its simpler crystal structure, high critical current densities J_c, high upper critical magnetic field, H_{c2}, transparent grain boundaries to supercurrent and low anisotropy make this material preferable to high-temperature (HTS) as well as conventional low temperature superconductors (LTS) [2]. The lower cost and ease of synthesis are the added advantages of this material. One of the concerns of using polycrystalline MgB_2 for technological application is its deteriorating superconducting properties at high-fields due to weak pinning [3,4]. Many groups have reported J_c values as high as $\sim 10^7$ A/cm^2 in the absence of an applied magnetic field at 5 K and $\sim 10^4$ A/cm^2 at 4.5 T and 5 K [5–7]. Many approaches have been employed to introduce effective pinning sites to improve the $J_c(H)$ behavior of MgB_2. It has been well studied that the introduction of grain boundaries, voids, crystal defects, dislocations, strain, impurity phases and nanophase inclusions into the superconductor provides very effective pinning sites. In this regard, many efforts have been made to improve the in-field superconducting properties of MgB_2. Many studies have shown that the lattice defects created by substitutions at Mg and B-sites can lead to improved H_{c2} and $J_c(H)$. Among the dopants, boron substitution with carbon in the form of carbon [8–10] and carbon nanostructures [11–15] is reported to improve J_c significantly at high magnetic fields. Also many carbon containing compounds [16–20] are reported to have enhanced H_{c2} and J_c. Carbon doping for B induces a crystal lattice distortion, especially in the boron plane, thus giving rise to strong intra-band scattering in the σ-band [21,22] which improves the pinning properties of MgB_2. One problem with C doping for B is the reduction in T_c [9]. However, it has been reported that the effect of C doping on T_c depends on various factors which include processing technique and the precursor materials used [23]. Recently, carbon doping in the form of graphene [24,25] has been reported to improve J_c considerably by increasing mainly the grain connectivity without affecting the value of T_c. Furthermore, magnetic elements when doped into MgB_2 are reported to suppress superconductivity in MgB_2 due the pair-breaking effect [26]. Nevertheless, rare-earth (RE) elements which also possess strong magnetic moments, are found not to suppress superconductivity in MgB_2 but rather favoring it by being present in the materials as efficient pinning sites [27,28]. It has been reported that with the introduction of RE

* Corresponding author. Tel.: +91 1332 285353; fax: +91 1332 273560.
E-mail address: gdvarfph@iitr.ernet.in (G.D. Varma).

oxides into the MgB_2, J_c is improved in the range of low and medium magnetic fields. The effect of RE elements addition in MgB_2 has been studied intensively, but there is still a requirement to explore the possible approaches to improve J_c in the entire magnetic field range. In this paper, we have done a thorough study of the effect of combined addition of graphene oxide (GO) and a series of RE oxides (REO, RE = La, Sm, Eu, Gd, Tb and Ho) on the superconducting properties of MgB_2. We have used a fixed value of 1 wt% REO for addition and the reported [25] optimum value 3 wt% for GO addition to get best $J_c(H)$ results. We observed that the critical current density, J_c and upper critical field $H_{c2}(0)$ improved significantly with GO + REO addition into MgB_2 samples with no significant change in critical temperature, T_c. The pinning mechanisms present in these samples are described and discussed in the present paper.

2. Experimental

In the present work, we have synthesized (i) pristine MgB_2, (ii) graphene oxide (GO, 3 wt%) added MgB_2, (iii) a series of rare-earth oxide, REO (1 wt%, RE = La, Sm, Eu, Gd, Tb and Ho) added MgB_2 and (iv) a series of GO (3 wt%) + REO (1 wt%) added MgB_2 samples using the standard solid state reaction route. The GO used for addition was synthesized in the laboratory using improved Hummer's method [29] as described in previous work [25], and REO used were purchased from Loba Chemie with 99.9% purity and submicron grain size. For the synthesis of samples, appropriate amounts of Mg (Sigma Aldrich, 99.9% pure) and B (Sigma Aldrich, amorphous, 99%) were mixed with required compositions of GO and REO (RE = La, Sm, Eu, Gd, Tb and Ho) in an agate mortar. In order to compensate for the Mg loss during sample synthesis, for all samples excess Mg (~5 wt%) was added [30,31]. The mixing of chemicals was done thoroughly for about an hour and after this the resulting powder was pressed into rectangular pellets. The pellets were placed in an iron tube and then sintered at 850 °C in reducing atmosphere of Ar/H_2 (9/1) for 3 h followed by slow cooling down to 650 °C and subsequently quenching to room temperature. Henceforth, the pristine, GO-added, REO added and (REO + GO) added MgB_2 samples will be represented as MB, MBG, MBR and MBRG (R = La_2O_3, Sm_2O_3, Eu_2O_3, Gd_2O_3, Tb_2O_3 and Ho_2O_3), respectively. The crystallographic structure of the samples was studied using X-ray diffractometry with Cu Kα radiation (1.5406 Å) over an angular (2θ) range between 10° and 80°. The morphological study of the samples was done using a field emission scanning electron microscope (FE-SEM) (FEI-QUANTA 200 FEG). The resistance measurement in different applied magnetic fields (0–8 T) was accomplished using a Physical Property Measurement System (PPMS) (Quantum Design-6000) at the University of Fribourg, Switzerland. The irreversibility fields, H_{irr}, and upper critical field, H_{c2} (T), were calculated using the criteria 10% and 90% of normal state resistivity, ρ_n for different applied fields, respectively. The DC magnetic measurements were carried out using a Superconducting Quantum Interference Device (SQUID) magnetometer (Quantum Design MPMS XL).

3. Results and discussion

From the XRD patterns (Fig. 1) the dominant phase in all the samples is MgB_2 along with small quantities of MgO and REB_x (x = 4 and 6, RE = La, Sm, Eu, Gd, Tb and Ho) impurity phases. The peaks corresponding to MgB_2 phase are indexed based on the hexagonal AlB_2-type (space group – $P6/mmm$), and the impurity phases MgO, REB_4 and REB_6 are marked by '*', '♦' and '#', respectively,0 as shown in Fig. 1. The appearance of MgO during the synthesis of MgB_2 samples is difficult to avoid due to the entrapped air before the tube is closed. The presence of oxide additives also adds oxygen during the sample preparation. We have calculated the volume percentage of MgO present in the samples using the formula: $X = \frac{\sum \text{peak intensities of impurity phase}}{\sum \text{peak intensities of impurity phase}} \times 100$, the obtained values are listed in Table 1. We observe that the amount of MgO in the samples added with GO and REO is larger than the pristine MgB_2 sample. The lattice parameters, a and c for all samples have been obtained from the refinement of XRD data using the X'pert HighScore software. The obtained values of a and c are shown in Table 1. We observe no significant change in the lattice parameters of MBG, MBR and MBRG samples as compared to pure MgB_2. This indicates that neither RE (=La, Sm, Eu, Gd, Tb and Ho) nor carbon from GO enter into the MgB_2 crystal lattice. From the XRD patterns, we see that for the MBG, MBR and MBRG samples the full width at half maxima (*FWHM*) of the MgB_2 peaks is enhanced as compared to the corresponding peaks of pristine MgB_2. The *FWHM* values of the (1 1 0) peak are listed in Table 1. and it can be seen that *FWHM* for the MBRG samples is larger than for the MBR samples. Since the *FWHM* values are influenced by the crystallite size and strain in the lattice, this result is indicative of an increased lattice strain in the MBRG samples [32]. The grain connectivity in the samples with the introduction of GO is also seen in the FESEM micrographs (see Fig. 2). Fig. 2 compares the FESEM micrographs of (a) MB, (b) MBG (inset shows the FESEM micrograph of GO powder), (c) MBR (R = Ho) and (d) MBRG (R = Ho). It reveals that the grain size decreases with REO-addition in the samples. This result is in conformity with the XRD result discussed above. The EDX analysis reveals the presence of all elements in the samples. We annealed the GO powder separately at 850 °C in Ar/H_2 (9/1) atmosphere and from XRD result we found that GO reduces to reduced-graphene oxide (rGO). It has been studied and found that the presence of rGO in the samples creates micro-strain which helps in improving the superconducting properties of the MgB_2 sample [14].

Fig. 3(a) and (b) shows the resistivity versus temperature plots for the MB, MBG, MBR and MBRG samples in the temperature range 30 K–300 K. To estimate the effect of introducing REO and GO additives on the sample quality and carrier scattering, we have calculated the value of the residual resistivity ratio, *RRR* (=ρ(300 K)/ρ(40 K)). The latter provides information about the sample quality in terms of the presence of impurities and lattice defects. Samples with relatively high RRR values are known to be of high quality [33]. In the present case, the *RRR* values for MBR samples have decreased as compared to pristine MgB_2. This is due to the presence of REB_x impurity phases which cause increased electron scattering and thus decrease the value of *RRR*. However, among the MBR samples, the *RRR* value remains almost unchanged; this is in line with the similar amounts of impurities that are present in these samples. In the case of the MBRG samples, the *RRR* values are even lower than that of the MBR samples. From the temperature dependence of the resistivity, we have also calculated the superconducting area fraction, $A_f = \Delta\rho_{ideal}/\Delta\rho$, $\Delta\rho = \rho(300\text{ K}) - \rho(40\text{ K})$ and $\Delta\rho_{ideal} = 7.3\ \mu\Omega$ cm [34], which has been proposed by Rowell [35] as a parameter to describe the strength of the impurity scattering. Here $\Delta\rho_{ideal}$ is the ideal value of $\Delta\rho$ for a fully connected system. The calculated values of A_f are listed in Table 1. According to Rowell's analysis, fully connected MgB_2 shows a well defined temperature dependent scattering which gives a characteristic change in ρ from 300 K to 40 K. We observe that A_f has increased with RE addition in the MgB_2 samples which is consistent with the earlier studies done with rare-earth oxide doping [27]. With addition of GO + REO in the MgB_2 samples, we see a further enhancement in the A_f values. This indicates that the connectivity is improved by the GO addition. From this result, an improvement in the J_c–H behavior can be expected.

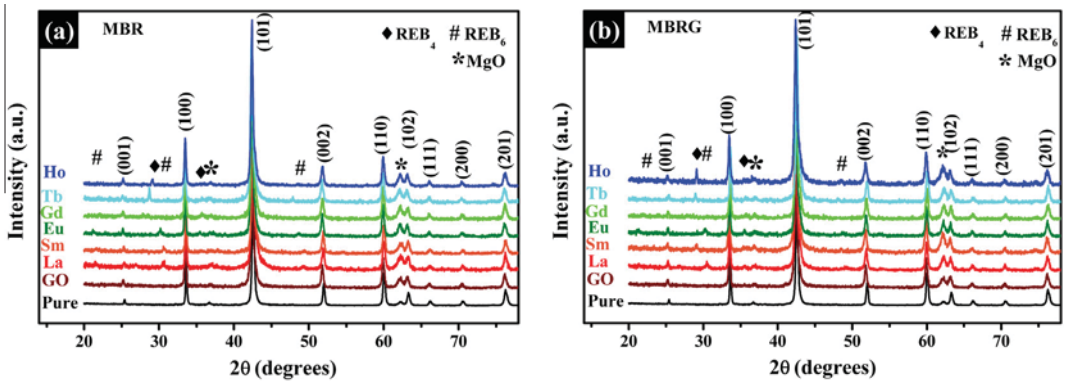

Fig. 1. X-ray diffraction patterns for pure MgB_2, GO-added, rare-earth added MgB_2, denoted as MBR (R = La, Sm, Eu, Gd, Tb and Ho) series and GO and rare-earth added MgB_2, denoted as MBRG (R = La, Sm, Eu, Gd, Tb and Ho) series of samples.

Table 1
Lattice parameters; *a* and *c*, *FWHM*, MgO content, critical temperature (T_c), *RRR*, A_f and $H_{c2}(0)$ for (a) MBR (MgB_2 + 1 wt% REO) and (b) MBRG (MgB_2 + 1 wt% REO + 3 wt% GO) samples.

Sample	*a* (Å)	*c* (Å)	FWHM (1 1 0)	MgO (%)	T_c (K)	RRR	A_f	H_{c2} (0) (T)
MB	3.0889	3.5339	0.137	2.24	38.76	3.14	0.19	17.0
MBG	3.0814	3.5277	0.144	3.33	38.75	2.73	0.23	17.5
(a)								
MBLa	3.0862	3.5271	0.148	4.21	38.80	2.77	0.20	19.6
MBSm	3.0845	3.5259	0.140	3.56	38.82	2.74	0.22	19.5
MBEu	3.0832	3.5239	0.144	4.48	38.77	2.86	0.19	18.9
MBGd	3.0840	3.5251	0.145	4.39	38.81	2.75	0.21	19.3
MBTb	3.0833	3.5240	0.138	4.60	38.77	2.88	0.20	19.8
MBHo	3.0840	3.5260	0.156	4.80	38.81	2.77	0.23	19.5
(b)								
MBLaG	3.0850	3.5256	0.152	5.10	39.00	2.80	0.24	19.9
MBSmG	3.0852	3.5257	0.152	4.80	39.12	2.78	0.29	20.8
MBEuG	3.0844	3.5253	0.159	3.78	38.82	2.82	0.29	21.4
MBGdG	3.0853	3.5261	0.156	4.29	38.82	2.71	0.24	21.0
MBTbG	3.0858	3.5262	0.151	3.70	38.82	2.84	0.27	22.4
MBHoG	3.0857	3.5280	0.174	4.95	38.61	2.60	0.31	20.5

The transition temperature, T_c for all the samples was determined from the onset of the superconducting transition in the resistivity versus temperature (ρ–T) curve in zero applied magnetic field. The values of T_c are shown in Table 1. It shows that with respect to the MB sample there is no significant drop in T_c of MBG, MBR and MBRG samples. This result is consistent with the unchanged lattice parameters of all the GO, REO and GO + REO added samples. From the magneto-resistivity measurements in applied fields in the range 0–8 T, we have calculated the values of the upper critical fields, H_{c2} using the criteria of $\rho(T, H_{c2}) = 0.9\text{-}\rho_n(T, H)$, where ρ_n is the value of resistivity in the normal state just before the superconductivity transition. The experimental data are plotted in Fig. 4(a) for samples MB, MBG and MBR; in Fig. 4(b) for samples MB, MBG and MBRG. Using the Ginzburg–Landau model [36], $H_{c2}(T) = H_{c2}(0)(1 - t^2)/(1 + t^2)$ we have calculated the upper critical fields at 0 K. The values of $H_{c2}(0)$ are listed in Table 1. The value of $H_{c2}(0)$ for the pure sample is 16.95 T in good agreement with the reported value [36]. The values of $H_{c2}(0)$ of the MBR samples are enhanced by ~2 T in comparison to MB. This improvement in $H_{c2}(0)$ is possibly due to decreased grain size of the MBR samples which arises due to the presence of REB_x (x = 4 and 6) precipitates at the grain boundaries. In case of the MBG sample, an improvement of ~1 T was observed for $H_{c2}(0)$. In the case of MBRG samples, we observed enhancement in $H_{c2}(0)$ of 4–5 T over the pristine MB sample. This enhancement of $H_{c2}(0)$ in MBRG samples is due to the lattice strain in the samples that is caused by the different thermal expansion coefficients of the MgB_2 matrix and rGO [14,24]. Irreversibility field, H_{irr} is calculated using the criteria of $\rho(T, H_{irr}) = 0.1\rho_n(T, H)$ and the values obtained are plotted in Fig. 4(c) for samples MB, MBG and MBR; Fig. 4(d) for samples MB, MBG and MBRG.

Fig. 5(a) and (b) show the magnetic hysteresis loops (M–H) for MBR (in the field range 1.5–7 T) and MBRG (in the field range −7 T to −1.5 T) at 10 K and 20 K, respectively. The M–H loops are not shown in the range lower than ±1.5 T, where all the samples show flux jump that are caused by a thermo-magnetic instability as reported previously in high-J_c samples [37]. From the plots, we see a considerable increase in $M(H)$ loop widths of MBRG samples as compared to the MB, MBG and MBR samples at 10 K and 20 K. This indicates an increased flux pinning strength in the samples and an improvement in the magnetic critical current density, $J_c(H)$ with the addition of GO + REO.

The magnetic field dependence of J_c of the samples has been estimated at 10 K and 20 K using the magnetization (M–H) curves following the Bean critical state model [38]: $J_c = 20\Delta M/[Va(1 - a/3b)]$, where $\Delta M = M(+) - M(-)$ in the positive applied field region of the M–H loop, V is the volume, a and b are the length and width, respectively, of the rectangular samples used for the magnetization measurements. The field dependence of J_c is shown in Fig. 6(a) and (b) at 10 K for the MBR series and MBRG series, respectively. The field dependence of J_c at 20 K is shown in the insets of Fig. 6(a) and (b) on a logarithmic scale for the MBR series and MBRG series, respectively. From Fig. 6(a) we clearly observe a significant improvement in J_c for the MBR samples as compared to the MB sample. The J_c

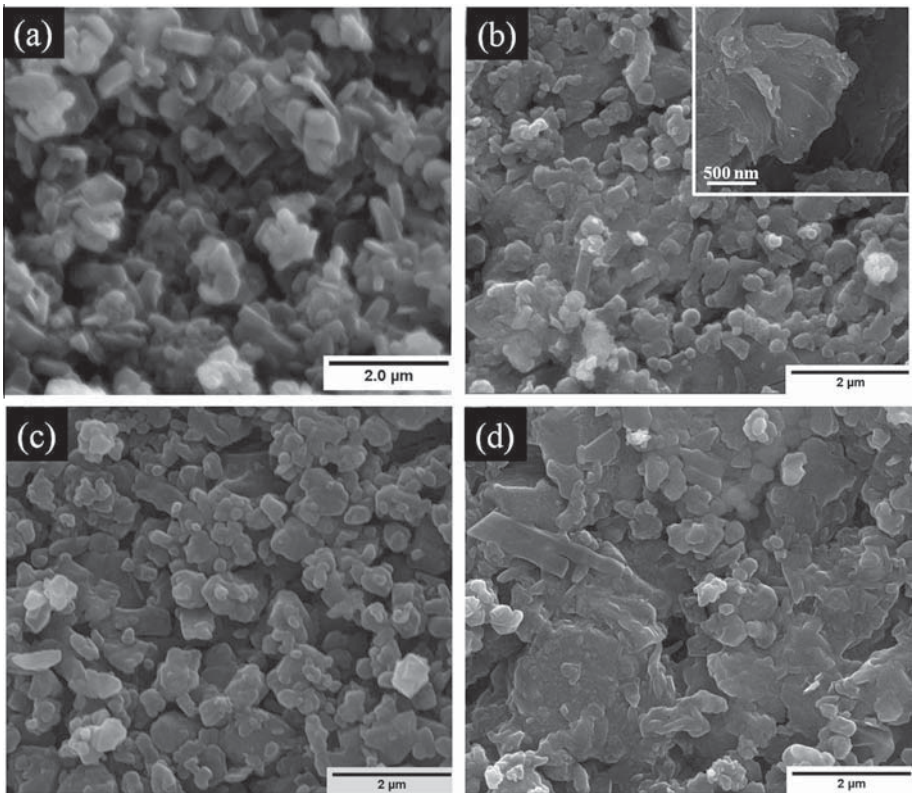

Fig. 2. FESEM micrographs for the (a) MB, (b) MBG, (c) MBR (R = Ho) and (d) MBRG (R = Ho) samples. The inset of (b) shows FESEM micrograph of GO powder used for addition.

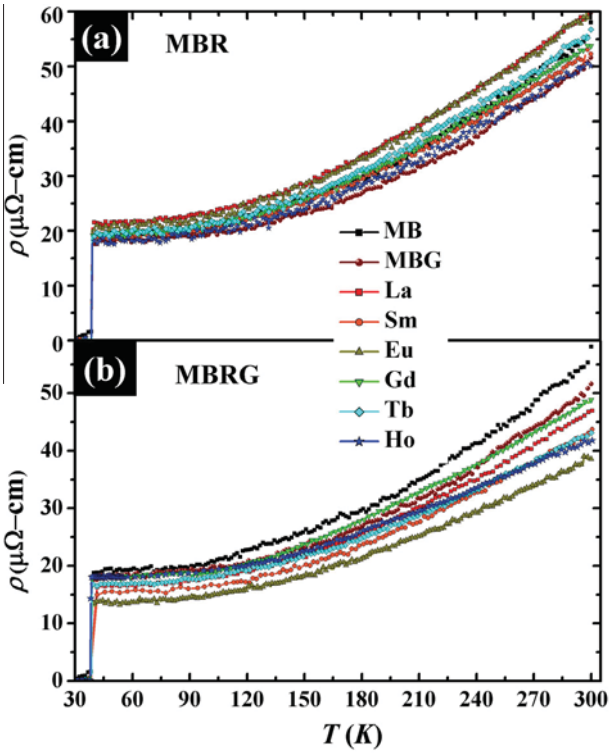

Fig. 3. (a) and (b) show the resistivity plot for MB, MBG, MBR and MBRG samples in the temperature range 30–300 K.

values are further enhanced (as shown in Fig. 6(b)) with addition of REO + GO in MgB_2. This is possibly due to the combined effect of addition of REO + GO in MgB_2. From the XRD results we have seen the presence of REB_x impurity phase in the REO + GO added MgB_2 samples (MBRG), which may act as strong pinning centres in the samples. Furthermore, in these samples we have seen improved grain connectivity due to addition of GO. Thus these two effects, i.e., enhanced flux pinning and improved grain connectivity, may be responsible for the improved $J_c(H)$ behavior of MBRG samples over the other studied samples. The values of J_c at low (1.5 T) and high field (5 T) corresponding to 10 K and 20 K are listed in Table 2. In case of the GO added sample (MBG), a significant improvement (6.7 times) over the pure MgB_2 sample has been observed as was reported earlier [25]. In the MBR samples also, we see improvements as large as ~12 times (for RE = Ho) at 1.5 T (10 K) in comparison to the pure sample. In case of the MBR samples we believe that the REB_x impurities give rise to the improved J_c values. On the other hand, in case of the MBG sample the improvement in J_c value is due to the improved grain connectivity and the micro-strain introduced into the MgB_2 matrix, as discussed above, which enhances the flux-pinning in the sample. Among the MBR samples it also appears that the enhancement of $J_c(H)$ scales with the magnitude of the magnetic moment of the added rare-earth elements. From the $J_c(H)$ plots of MBR samples, we see that the oxides of rare-earth elements of larger magnetic moment, like Tb, Ho, Gd, provide more efficient flux pinning centers. Fig. 6 and Table 2. show that in case of the MBRG samples there is a considerable improvement of $J_c(H)$ over that of the MBR and MBG samples (see Fig. 6). The maximum J_c values at 10 K are 9.59×10^5 A/cm^2 at 1.5 T and 4.66×10^4 A/cm^2 at 5 T of the MBRG (R = Tb) sample. This corresponds to a 23.3-fold improvement of J_c at 10 K and 5 T as compared to the pure MgB_2 sample. At higher temperature (20 K) we observe the highest J_c value of 5.02×10^5 A/cm^2 at 1.5 T for the MBRG (R = Tb) sample. These J_c values of the MBRG samples are comparable to the highest reported J_c results in the literature for SiC-doped MgB_2 samples [5,39].

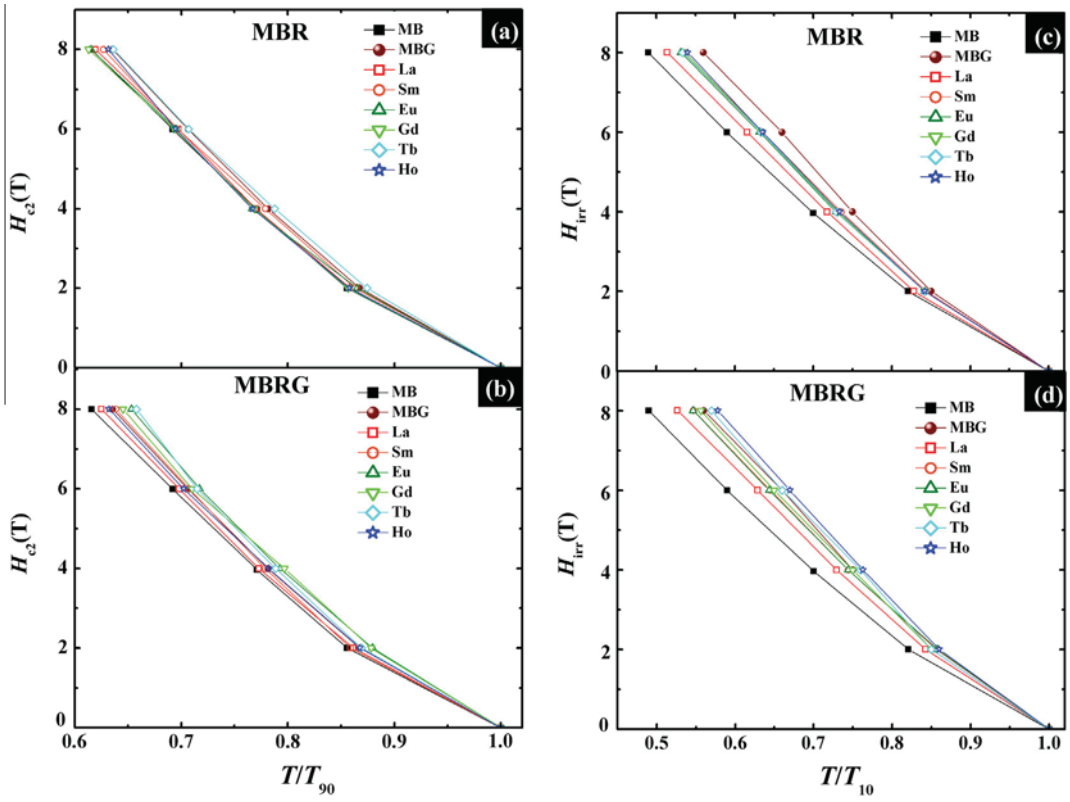

Fig. 4. (a) and (b) presents the H_{c2}(T) versus T/T_{90} (T_{90} is the temperature where the value of ρ is $0.9\rho_n$, ρ_n is the normal state resistivity) plots for the MB, MBG and MBR samples; and MB, MBG and MBRG samples, respectively. (c) and (d) presents the H_{irr}(T) versus T/T_{10} (T_{10} is the temperature where the value of ρ is $0.1\rho_n$, ρ_n is the normal state resistivity) plots for the MB, MBG and MBR samples; and MB, MBG and MBRG samples, respectively.

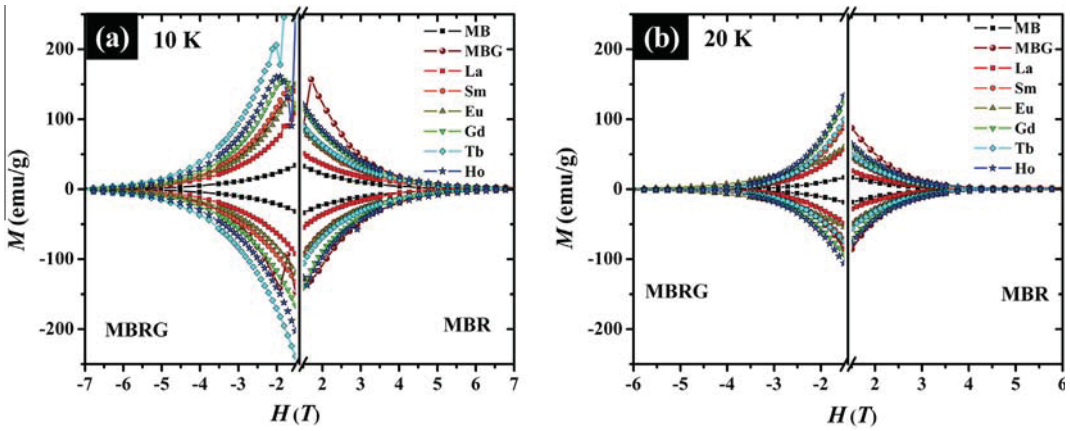

Fig. 5. Magnetic hysteresis loop for the RE-added (0–7 T) and RE and GO added (−7 to 0 T) samples at 10 K (a) and 20 K (b).

In order to understand the flux pinning mechanism in both series (MBR and MBRG) of samples, we have calculated the volume-pinning force density, F_p ($F_p = J_c(H) \times H$), from the $J_c(H)$ curves at 10 K. In Fig. 7(a) and (b), we have shown f_p ($=F_p/F_p^{max}$) versus the normalized applied magnetic field, h ($=H/H_{max}$) for the MBR and MBRG samples, respectively. Here, F_p^{max} is the maximum value of F_p at a particular temperature and H_{max} is the value of field corresponding to F_p^{max}. The values of F_p^{max} and H_{max} have been determined from the average shape of the f_p versus h plots, obtained by ignoring some flux jump points. The signatures of flux jumps at low fields are also observed here. In high temperature superconductors the normalized volume pinning force, f_p, often scales with H/H_{irr}. However, it is difficult to calculate the accurate value of H_{irr} from the dc magnetization measurements. In order to avoid this problem, the data are often scaled with H/H_{max} ($=h$) instead of H/H_{irr} [40], as is done in the present case. The scaling for $f(h)$ is often done with the help of following equations [40–42] for the different flux pinning mechanisms:

$$f_p = 3h^2\left(1-\frac{2h}{3}\right), \quad \delta k\text{-pinning} \tag{1}$$

$$f_p = \frac{9}{4}h\left(1-\frac{h}{3}\right)^2, \quad \delta T_c\text{-pinning} \tag{2}$$

$$f_p = \frac{25}{16}\sqrt{h}\left(1-\frac{h}{5}\right)^2, \quad \text{surface-pinning} \tag{3}$$

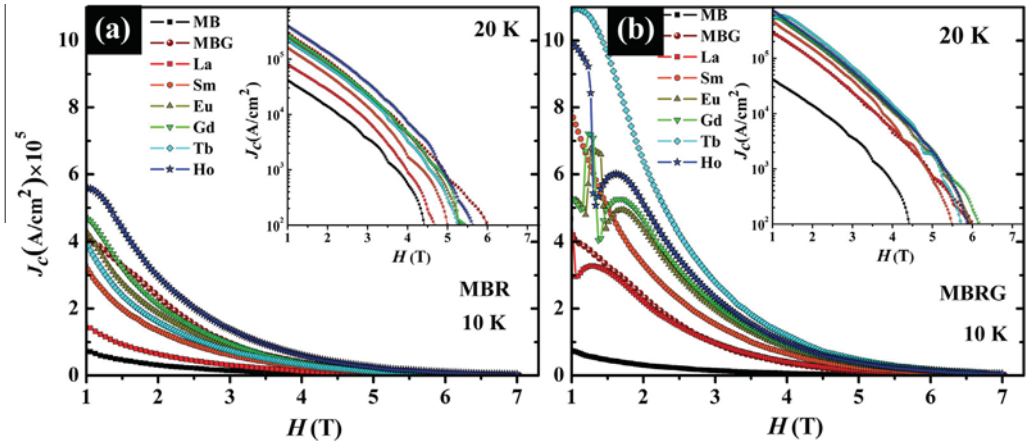

Fig. 6. (a) and (b) Magnetic field dependent critical current, J_c, at 10 K (the inset shows $J_c(H)$ at 20 K on a logarithmic scale) for RE-added and RE and GO added samples, respectively.

Table 2
Critical current density, J_c, at 10 K and 20 K in magnetic fields of 1.5 T and 5 T.

Sample (RE)	J_c (A/cm^2)				Sample (GO + RE)	J_c (A/cm^2)			
	10 K		20 K			10 K		20 K	
	1.5 T ($\times10^5$)	5 T ($\times10^3$)	1.5 T ($\times10^5$)	4 T ($\times10^3$)		1.5 T ($\times10^5$)	5 T ($\times10^3$)	1.5 T ($\times10^5$)	4 T ($\times10^3$)
MB	0.4	2.0	0.2	0.5	MB	0.4	2.0	0.2	0.5
MBG [25]	3.3	13.5	1.7	4.6	MBG	3.3	13.5	1.7	4.6
MBLa	1.0	5.0	0.5	1.8	MBLaG	3.1	16.2	1.7	5.4
MBSm	2.0	9.6	1.0	0.7	MBSmG	4.9	33.1	3.5	10.8
MBEu	2.8	15.1	1.6	4.6	MBEuG	5.0	24.0	2.6	6.7
MBGd	3.2	16.5	1.6	4.7	MBGdG	5.0	36.5	3.8	11.9
MBTb	2.4	12.5	1.3	3.3	MBTbG	9.6	46.6	5.0	14.2
MBHo	4.4	24.9	2.3	7.3	MBHoG	5.9	39.8	4.1	12.3

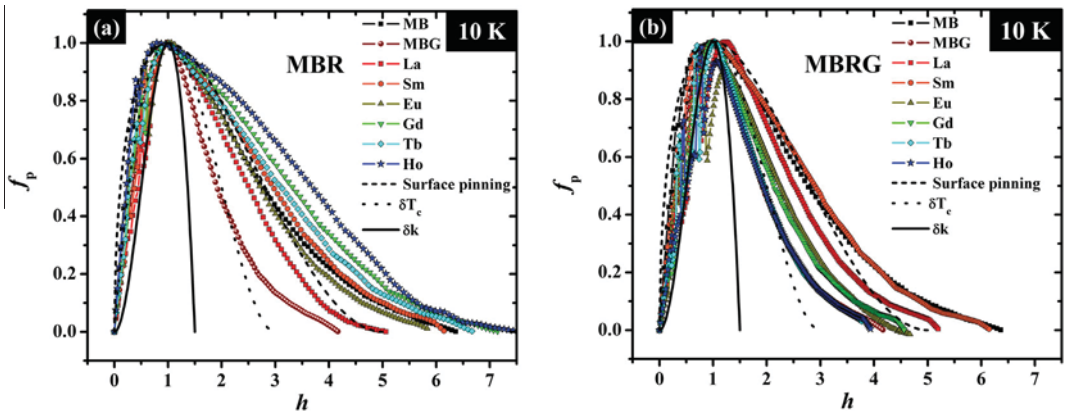

Fig. 7. Normalized flux pinning force density, F_p/F_p^{max} at 10 K for (a) MBR and (b) MBRG samples.

In both series of samples, MBR and MBRG, the scaling suggests that the dominant pinning mechanism in the pure and MBR samples is related to surface pinning or to grain boundaries, while in the GO added sample we observe that the δT_c or point-pinning is the dominant one. However, in the MBRG samples we see that the f_p curve shift towards the point-pinning. This suggests that the GO-added MgB_2 sample has enhanced point pinning mechanism.

In comparison to the previous studies done with co-doping of rare-earth oxide and carbon sources, e.g. graphite [16] and SiC [6], it is clear from the present study that GO is a better source of carbon to be added along with rare-earth oxides in MgB_2. In the previous studies, the J_c has improved in the region of high field, while in the present case there is improvement in J_c in the entire magnetic field range (0–7 T) without affecting the critical temperature, T_c. At the synthesis temperature, although GO does not dissociate to give C for lattice substitution, but it helps in improving the grain connectivity, i.e. provide easy path for the flow of superconducting current. We have also observed from the $J_c(H)$ behaviors of MBR and MBRG samples that the additions of oxides of rare earth elements with higher magnetic moment are more effective in improving flux pinning and thus $J_c(H)$.

4. Conclusion

In the present work, we have systematically investigated the effect of addition of (i) graphene oxide (GO), (ii) a series of

rare-earth (RE, RE = La, Sm, Eu, Gd, Tb and Ho) oxides (REO) and (iii) a mixture of GO and rare-earth oxides (GO + REO) on the superconducting properties of the MgB_2 superconductor. We have observed that the REO addition introduces effective pinning centers that lead to an improved critical current density. The introduction of GO in the MgB_2 matrix leads to an improvement in the grain connectivity which also plays an important role in improving the critical current density. The combined addition of REO and GO in the MgB_2 superconductor has significantly improved J_c in the entire magnetic field regime from 0 to 7 T, without affecting T_c. The dominant pinning mechanism in the MBR samples is the surface or grain-boundary pinning, while in the MBG sample, it is the point-pinning. In the MBRG samples, the pinning contribution comes both from grain boundary and point pinning.

Acknowledgments

One of the authors, Sudesh is thankful to Ministry of Human Resources and Development (MHRD, Govt. of India), for providing the financial support. S. Das and C. Bernhard acknowledge funding by the Swiss National Science Foundation (SNF) Grant No. 200020-140225 and by Project No. 122935 of the Indo-Swiss Joint Research Program (ISJRP).

References

[1] J. Nagamatsu, N. Nakagawa, T. Muranaka, Y. Zenitani, J. Akimitsu, Nature 410 (2001) 63–64, http://dx.doi.org/10.1038/35065039.
[2] D.C. Larbalestier, L.D. Cooley, M.O. Rikel, A.A. Polyanskii, J. Jiang, S. Patnaik, et al., Nature 410 (2001) 186–189, http://dx.doi.org/10.1038/35065559.
[3] Y. Bugoslavsky, G.K. Perkins, X. Qi, L.F. Cohen, A.D. Caplin, Nature 410 (2001) 563–565, http://dx.doi.org/10.1038/35069029.
[4] Y. Bugoslavsky, L.F. Cohen, G.K. Perkins, M. Polichetti, T.J. Tate, R. Gwilliam, A.D. Caplin, Nature 411 (2001) 561–563, http://dx.doi.org/10.1038/35079024.
[5] K.S.B. De Silva, X. Xu, X.L.L. Wang, D. Wexler, D. Attard, F. Xiang, S.X.X. Dou, K.S.B. De Silva, Scr. Mater. 67 (2012) 802–805, http://dx.doi.org/10.1016/j.scriptamat.2012.07.014.
[6] N. Varghese, K. Vinod, M.K. Chattopadhyay, S.B. Roy, U. Syamaprasad, J. Appl. Phys. 107 (2010) 013907, http://dx.doi.org/10.1063/1.3275504.
[7] C. Shekhar, R. Giri, R.S. Tiwari, D.S. Rana, S.K. Malik, O.N. Srivastava, Supercond. Sci. Technol. 18 (2005) 1210–1214, http://dx.doi.org/10.1088/0953-2048/18/9/011.
[8] A.K. Bengtson, C.W. Bark, J. Giencke, W. Dai, X. Xi, C.-B. Eom, D. Morgan, J. Appl. Phys. 107 (2010) 023902, http://dx.doi.org/10.1063/1.3275867.
[9] W. Mickelson, J. Cumings, W. Han, A. Zettl, Phys. Rev. B. 65 (2002) 052505, http://dx.doi.org/10.1103/PhysRevB.65.052505.
[10] C. Shekhar, R. Giri, R.S. Tiwari, O.N. Srivastava, S.K. Malik, J. Appl. Phys. 102 (2007) 093910, http://dx.doi.org/10.1063/1.2805650.
[11] Q. Cai, Y. Liu, Z. Ma, D.A. Cardwell, Physica C 492 (2013) 6–10, http://dx.doi.org/10.1016/j.physc.2013.05.002.
[12] W. Gruner, M. Herrmann, A. Nilsson, H. Hermann, W. Häßler, B. Holzapfel, Supercond. Sci. Technol. 20 (2007) 601–606, http://dx.doi.org/10.1088/0953-2048/20/7/003.
[13] G. Pasquini, A. Serquis, A.J. Moreno, G. Serrano, L. Civale, J. Appl. Phys. 114 (2013) 023907, http://dx.doi.org/10.1063/1.4813132.
[14] K.S.B. De Silva, S. Gambhir, X.L. Wang, X. Xu, W.X. Li, D.L. Officer, D. Wexler, G.G. Wallace, S.X. Dou, J. Mater. Chem. 22 (2012) 13941, http://dx.doi.org/10.1039/c2jm30323j.
[15] A. Gupta, A.V. Narlikar, Supercond. Sci. Technol. 22 (2009) 125029, http://dx.doi.org/10.1088/0953-2048/22/12/125029.
[16] N. Ojha, V.K. Malik, R. Singla, C. Bernhard, G.D. Varma, Supercond. Sci. Technol. 23 (2010) 045005, http://dx.doi.org/10.1088/0953-2048/23/4/045005.
[17] W.K. Yeoh, S.X. Dou, Physica C 456 (2007) 170–179, http://dx.doi.org/10.1016/j.physc.2007.01.024.
[18] M.S.A. Hossain, C. Senatore, R. Flukiger, M.A. Rindfleisch, M.J. Tomsic, J.H. Kim, S.X. Dou, Supercond. Sci. Technol. 22 (2009) 095004, http://dx.doi.org/10.1088/0953-2048/22/9/095004.
[19] C.M. Lee, S.M. Hwang, K. Sung, S.M. Lee, J. Joo, W.N. Kang, et al., IEEE Trans. Appl. Supercond. (2010) 1–4.
[20] Y.J. Kim, B.-H. Jun, K.S. Tan, B.G. Kim, J.M. Sohn, C.-J. Kim, Physica C 468 (2008) 1372–1374, http://dx.doi.org/10.1016/j.physc.2008.05.059.
[21] M. Angst, S. Bud'ko, R. Wilke, P. Canfield, Phys. Rev. B 71 (2005) 144512, http://dx.doi.org/10.1103/PhysRevB.71.144512.
[22] A. Sologubenko, N. Zhigadlo, S. Kazakov, J. Karpinski, H. Ott, Phys. Rev. B 71 (2005) 020501, http://dx.doi.org/10.1103/PhysRevB.71.020501.
[23] R.H.T. Wilke, S.L. Bud'ko, P.C. Canfield, D.K. Finnemore, S.T. Hannahs, Physica C 432 (2005) 193–205, http://dx.doi.org/10.1016/j.physc.2005.08.007.
[24] X. Xu, S.X. Dou, X.L. Wang, J.H. Kim, J.A. Stride, M. Choucair, W.K. Yeoh, R.K. Zheng, S.P. Ringer, Supercond. Sci. Technol. 23 (2010) 085003, http://dx.doi.org/10.1088/0953-2048/23/8/085003.
[25] Sudesh, N. Kumar, S. Das, C. Bernhard, G.D. Varma, Supercond. Sci. Technol. 26 (2013) 095008, http://dx.doi.org/10.1088/0953-2048/26/9/095008.
[26] X.F. Pan, T.M. Shen, G. Li, C.H. Cheng, Y. Zhao, Phys. Status Solidi 204 (2007) 1555–1560, http://dx.doi.org/10.1002/pssa.200622505.
[27] N. Ojha, V.K. Malik, C. Bernhard, G.D. Varma, Physica C 469 (2009) 846–851, http://dx.doi.org/10.1016/j.physc.2009.05.014.
[28] X.F. Pan, C.H. Cheng, Y. Zhao, J. Supercond. Nov. Magn. 24 (2010) 1611–1616, http://dx.doi.org/10.1007/s10948-010-1066-4.
[29] D.C. Marcano, D.V. Kosynkin, J.M. Berlin, A. Sinitskii, Z. Sun, A. Slesarev, L.B. Alemany, W. Lu, J.M. Tour, ACS Nano 4 (2010) 4806–4814, http://dx.doi.org/10.1021/nn1006368.
[30] A. Serquis, L. Civale, J.Y. Coulter, D.L. Hammon, X.Z. Liao, Y.T. Zhu, et al., Supercond. Sci. Technol. 17 (2004) L35–L37, http://dx.doi.org/10.1088/0953-2048/17/10/L01.
[31] Y.F. Wu, Y.F. Lu, J.S. Li, S.K. Chen, G. Yan, M.H. Pu, C.S. Li, P.X. Zhang, Physica C 467 (2007) 38–42, http://dx.doi.org/10.1016/j.physc.2007.08.010.
[32] J.H. Kim, S.X. Dou, J.L. Wang, D.Q. Shi, X. Xu, M.S.A. Hossain, W.K. Yeoh, S. Choi, T. Kiyoshi, Supercond. Sci. Technol. 20 (2007) 448–451, http://dx.doi.org/10.1088/0953-2048/20/5/007.
[33] T. Matsushita, M. Kiuchi, A. Yamamoto, J. Shimoyama, K. Kishio, Supercond. Sci. Technol. 21 (2008) 015008, http://dx.doi.org/10.1088/0953-2048/21/01/015008.
[34] J. Jiang, B.J. Senkowicz, D.C. Larbalestier, E.E. Hellstrom, Supercond. Sci. Technol. 19 (2006) L33–L36, http://dx.doi.org/10.1088/0953-2048/19/8/L02.
[35] J.M. Rowell, Supercond. Sci. Technol. 16 (2003) R17–R27.
[36] I.N. Askerzade, A. Gencer, N. Guclu, Supercond. Sci. Technol. 15 (2002) L13–L16.
[37] V. Sandu, G. Aldica, S. Popa, P. Badica, E. Cimpoiasu, F. Dumitrache, E. Sandu, J. Appl. Phys. 110 (2011) 123921, http://dx.doi.org/10.1063/1.3672820.
[38] C.P. Bean, Rev. Mod. Phys. 36 (1964) 31.
[39] J.H. Kim, S. Zhou, M.S.A. Hossain, A.V. Pan, S.X. Dou, Appl. Phys. Lett. 89 (2006) 142505, http://dx.doi.org/10.1063/1.2358947.
[40] T. Higuchi, S.I. Yoo, Phys. Rev. B 59 (1999) 1514–1527.
[41] I. Shigeta, T. Abiru, K. Abe, A. Nishida, Y. Matsumoto, Physica C 392–396 (2003) 359–363, http://dx.doi.org/10.1016/S0921-4534(03)01049-9.
[42] Z.X. Shi, Y.X. Zhang, H. Lv, M. Xu, E.-M. Choi, S.-I. Lee, Physica C 467 (2007) 101–105, http://dx.doi.org/10.1016/j.physc.2007.09.012.